Microchimica Acta (2023) 190:237
https://doi.org/10.1007/s00604-023-05818-8

ORIGINAL PAPER

Large-scale fabrication of ion-selective electrodes for simultaneous detection of Na^+, K^+, and Ca^{2+} in biofluids using a smartphone-based potentiometric sensing platform

Kanyapat Teekayupak[1] · Atchara Lomae[2] · Ismail Agir[3] · Natthaya Chuaypen[4] · Thasinas Dissayabutra[4] · Charles S. Henry[2,5] · Orawon Chailapakul[1] · Tugba Ozer[1,2,6,7] · Nipapan Ruecha[1,2]

Received: 15 March 2023 / Accepted: 25 April 2023 / Published online: 24 May 2023

Abstract

A significant bottleneck exists for mass-production of ion-selective electrodes despite recent developments in manufacturing technologies. Here, we present a fully-automated system for large-scale production of ISEs. Three materials, including polyvinyl chloride, polyethylene terephthalate and polyimide, were used as substrates for fabricating ion-selective electrodes (ISEs) using stencil printing, screen-printing and laser engraving, respectively. We compared sensitivities of the ISEs to determine the best material for the fabrication process of the ISEs. The electrode surfaces were modified with various carbon nanomaterials including multi-walled carbon nanotubes, graphene, carbon black, and their mixed suspensions as the intermediate layer to enhance sensitivities of the electrodes. An automated 3D-printed robot was used for the drop-cast procedure during ISE fabrication to eliminate manual steps. The sensor array was optimized, and the detection limits were 10^{-5} M, 10^{-5} M and 10^{-4} M for detection of K^+, Na^+ and Ca^{2+} ions, respectively. The sensor array integrated with a portable wireless potentiometer was used to detect K^+, Na^+ and Ca^{2+} in real urine and simulated sweat samples and results obtained were in agreement with ICP-OES with good recoveries. The developed sensing platform offers low-cost detection of electrolytes for point-of-care applications.

Keywords Ion-selective electrode · Mass-production · Point-of-care diagnosis · Carbon nanomaterial · Wireless detection

Introduction

Urine and sweat have gained more importance for clinical analysis especially for infants and elderly people to reduce the need for blood sampling [1]. Urine and sweat both provide physiological information about personal health conditions via noninvasive and painless assessment of electrolytes, metabolites, and proteins [2]. Na^+, K^+, and Ca^{2+} are the most important ions, and their concentrations are closely regulated in biological fluids [3]. For Ca^{2+}, its imbalances

✉ Orawon Chailapakul
corawon@chula.ac.th

✉ Tugba Ozer
tozer@yildiz.edu.tr

✉ Nipapan Ruecha
nipapan.r@chula.ac.th

1 Electrochemistry and Optical Spectroscopy Center of Excellence (EOSCE), Department of Chemistry, Faculty of Science, Chulalongkorn University, Bangkok 10330, Thailand

2 Metallurgy and Materials Science Research Institute, Chulalongkorn University, Bangkok 10330, Thailand

3 Department of Bioengineering, Faculty of Engineering and Natural Sciences, Istanbul Medeniyet University, Istanbul 34700, Türkiye

4 Metabolic Disease in Gastrointestinal and Urinary System Research Unit, Department of Biochemistry, Faculty of Medicine, Chulalongkorn University, Bangkok 10330, Thailand

5 School of Biomedical Engineering, Department of Chemistry, Colorado State University, Fort Collins, CO 80523, USA

6 Department of Bioengineering, Faculty of Chemical-Metallurgical Engineering, Yildiz Technical University, Istanbul 34220, Türkiye

7 Health Biotechnology Joint Research and Application Center of Excellence, Esenler, Istanbul 34220, Türkiye

causes chronic kidney diseases and mineral bone disorder [4]. While excess K^+ (hyperkalemia) leads to chronic renal failure, hypoaldosteronism, rhabdomyolysis, and cardiac arrhythmias [5], high Na^+ (hypernatremia) levels are associated with cystic fibrosis [6]. Although short-term freezing of urine can be used for electrolyte analysis, urine specimens should be analyzed immediately to obtain the most accurate results [7]. Therefore, in-situ analysis of Na^+, K^+, and Ca^{2+} in biofluids is needed.

All-solid-state ion-selective electrodes (ISEs) with a thin polymer membrane have been widely used in clinical applications due to their features such as portability, low-energy consumption, low-cost, and miniaturization [8, 9]. In addition, carbon-based materials as an intermediate layer modified between the conductive substrate and ion-selective membrane (ISM) have been proposed. The physical and chemical properties of the carbon-based materials provide a high electric charge capacity, leading a high stability of the sensor [10, 11]. Moreover, the high hydrophobicity of the carbon-based materials can eliminate the problem of water layer formation. These characteristics are the main requirements for the materials used as intermediate layers. Among the carbon-based materials, carbon black (CB) [12, 13], multi-walled carbon nanotubes (MWCNTs) [14], and graphene [15] have been successfully applied.

Various printing techniques including inkjet printing, screen printing, and 3D-printing have been used to simplify the carbon-based electrode fabrication. On the other hand, the fabrication process of the all-solid-state ISEs are labor- and time-intensive, and manual modification steps of the electrode surfaces can result in defects on electrode surface and reproducibility issues [16]. For point-of-care (POC) home-tests, either automatic calibration of ISEs or calibration-free ISEs should be developed for untrained end-users. In addition, low-cost portable sensing devices are required for frequent POC analysis. Therefore, simplification of manufacturing and calibration processes for ISEs is necessary.

Laser-induced graphene electrodes (LIGEs) have recently drawn attention due to their fast fabrication process and ability for mass-production [17, 18]. Lee et al. reported LIGEs for detection of K^+ and Na^+ ions [19]. Polydimethylsiloxane (PDMS)-lignin composite substrate was synthesized and used to fabricate electrodes via laser direct writing. Although the ISEs showed good sensitivity, their manufacturing procedure require synthesis of the substrate and manual drop-cast steps. Moreover, the system lack portability, limiting its use at the POC. In a recent study, Liao et al. developed LIGEs fabricated on polyimide substrate and modified with poly(3,4-ethylene dioxythiophene):polystyrene sulfonate (PEDOT:PSS) to simultaneously detect pH, Na^+, and K^+ levels in sweat with sensitivities of 51.5 mV/decade, 45.4 mV/decade, and 43.3 mV/decade, respectively [20]. Although the synthesis of substrate is not necessary for fabrication of LIGEs due to the use of commercially available polyimide substrate, the ISEs had low stability because of the presence of PEDOT:PSS as an intermediate layer, which is adversely affected by light and dissolved O_2 and CO_2 [21]. In addition, the fabrication process of these ISEs requires various manual steps. Therefore, LIGEs should be modified with stable nanomaterials to improve stability and sensitivities of the ISEs.

In this study, we used polyvinyl chloride (PVC), polyethylene terephthalate (PET) and polyimide (PI) as substrates for fabricating ISEs using stencil printing, screen printing and laser engraving, respectively. We compared sensitivities of the ISEs to determine the best material for fabrication process of the ISEs. The electrode surfaces were modified with various carbon nanomaterials including multi-walled carbon nanotubes (MWCNTs), graphene (GR), carbon black (CB), and their mixed suspensions for optimization of the intermediate layer to enhance sensitivities of the electrodes and evaluated LIGEs surfaces morphology by Fourier-transform infrared spectroscopy (FTIR), a field emission scanning electron microscope with energy dispersive X-ray spectrometer (FESEM-EDS), surface roughness, contact angle and their electrochemical and material properties.

To the best of our knowledge, this is the first report that presents a mass-produced laser-induced ISEs array via fully-automated fabrication and modification processes for simultaneous detection of Na^+, K^+ and Ca^{2+} ions. In addition, the effect for ISEs fabrication including substrate and carbon (nano)materials types were investigated and compared for the first time to achieve the best electrochemical performances. The carbon-based materials suspensions and ISMs were automated drop-cast by a low-cost (< $100) 3D-printed liquid handling robot (A3DMR) [22]. The sensing platform includes Internet-of-Things (IoT) enabled portable printed-circuit board (PCB) hardware part and custom software for wireless data transmission and storage to a smartphone during online monitoring. The low-cost (< $25) potentiometric device can perform automated calibration for the ISEs and display concentrations of the analytes on an OLED screen of the device [23]. As a proof of concept, the developed laser–induced ISEs were applied to clinical samples. The system offers rapid and fully automated mass-production of the ISEs for simultaneous detection of Na^+, K^+ and Ca^{2+} ions at the POC.

Experimental section

The details of chemical and materials, WISETIC platform, electrochemical measurements, characterization of surface morphology, and urine sample preparation are presented in Supplementary S1, S2, S3, and S4, respectively.

Preparation of solid-contact materials

The carbon-based materials including CB, MWCNTs, GR, and the CB mixtures either with MWCNT or GR as additives were prepared immediately prior to use by dispersing the carbon materials in THF and mixed for two min. Nine suspensions were obtained by the carbon materials: (1) 5 mg mL^{-1} CB, (2) 5 mg mL^{-1} MWCNT, (3) 5 mg mL^{-1} GR, (4) 0.2:1 MWCNT:CB, (5) 0.6:1 of MWCNT:CB, (6) 1:1 of MWCNT:CB, (7) 0.2:1 of GR:CB, (8) 0.6:1 of GR:CB, and (9) 1:1 of GR:CB in 1 mL of THF. The obtained materials are denoted as CB-ISE, MWCNTs-ISE, GR-ISE, respectively.

Preparation of ion-selective and reference membranes

The ion-selective membranes (ISMs) were prepared according to our recent reports [24]. Na ionophore X (1%, w/w), NaTFPB (0.9%, w/w), (65.7%, w/w) DOS, and PVC (32.4%, w/w) were mixed for Na^+-ISE. Valinomycin (2%, w/w), KTClPB (0.6%, w/w), DOS (64.7%, w/w), and high molecular weight PVC (32.7%, w/w) were mixed for K^+-ISE. To prepare the Ca^{2+}-ISE, the membrane cocktail including calcium ionophore II (ETH129) (2%, w/w), KTClPB (0.6%, w/w), PVC (32.5%, w/w), and NPOE (64.9%, w/w) was prepared. The additional components of Ca^{2+}-ISM for comparison are shown in Table S1. These ISM compositions were selected based on our previous reports and the literature [13, 23–26]. 200 mg of the membrane cocktails were dissolved in 1.5 mL of THF and sonicated for 15 min.

The reference membrane was prepared according to our previous procedure [24]. Briefly, the reference membrane cocktail was prepared using 200 mg poly(butyl methacrylate-co-methyl methacrylate), 68 mg KCl, and 5 mg tetradodecylammonium tetrakis(4 chlorophenyl)borate in 1 mL THF.

Fabrication of the all-solid-state ISEs and RE

Polyethylene terephthalate (PET), polyvinyl chloride (PVC) and polyimide (PI) substrates were used for fabrication of electrodes via three different techniques. While TC303 graphite and carbon ink were mixed at 0.6:1 w/w ratio to apply on PET substrate via in-house stencil printing, PVC substrate was used for screen-printing using carbon ink, and dried in an oven at 60 °C for 30 min. A laser scribing micromachining system with a semiconductor diode laser (Robotech LRT2030, Ideamaker Technology, Thailand) controlled by a computer was used to fabricate a LIGE. A high-temperature laser was used to obtain the carbon-containing PI-based electrodes via combustion and carbonization. Both of combustion and carbonization processes involve the conversion of sp^3 hybridized carbon atoms of the substrates to sp^2 hybridization of graphene. This conversion takes place via breaking of the C – O, C = O, and C – N bonds due to high temperature during laser process and aromatic compounds are then rearranged to form multilayer graphene [27]. The fabrication process of LIGE is shown in Video S1. The obtained electrodes were prepared by drop-casting 1.5 µL of the carbon-based materials twice as intermediate layer and dried in room temperature for 1 h. Then, the modified electrodes were drop-casted by 2 µL of the ISM cocktail three times as all-solid-state ISEs. The pipet tip was changed between each drop-cast of different type of ISM cocktails including Na^+-ISM, K^+-ISM, and Ca^{2+}-ISM to avoid contamination while 3D-printed robot was operated. After that, the ISEs were left in a desiccator overnight to let THF evaporate. The Na^+-ISE, K^+-ISE, and Ca^{2+}-ISE were conditioned in 10^{-1} M NaCl, 10^{-1} M KCl, and 10^{-2} M $CaCl_2$ for overnight, respectively.

For all-solid-state reference electrode (RE), the Ag/AgCl ink was applied on electrode surface and baked at 60 °C in an oven for 10 min. Then, 2 µL of reference membrane solution was drop-casted on the Ag/AgCl electrode three times and dried overnight in a desiccator. After that, the all-solid-state RE was conditioned in 3 M KCl for 16 h prior to analysis for further experiments.

Microfluidic device preparation

After ISE preparation, the microfluidic device was fabricated using the PET-double side adhesive tape (thickness 100 µm) and transparency film (thickness 100 µm) by laser-cutter, generating the flow channel as illustrated in Fig. 1. Then, the ISE electrode, PET-double side adhesive tape and the transparency film were sequentially assembled for creating the microfluidic device-based ISE. The device was used as non-invasive wearable sensors to directly attach to the human skin for collecting a sweat sample through the nine sample inlet holes (4 mm) for sample collection. Sweat sample was then flow through microfluidic channel (diameter 3 mm, length 5 mm) straightforward to the detection zone with a diameter of 15 mm. After the sweat sample was filled in detection zone, the multi-ions were measured using potentiometric technique. A small hole (1 mm diameter) placed in the middle of the transparency sheet was designed to remove air bubble in the microfluidic device during its operation. The fluidic operation of the LIGE is shown in Video S2.

Results and discussion

Optimization of ISM compositions

According to our previous study [28], we initially used CB-modified electrodes fabricated on PET substrate to

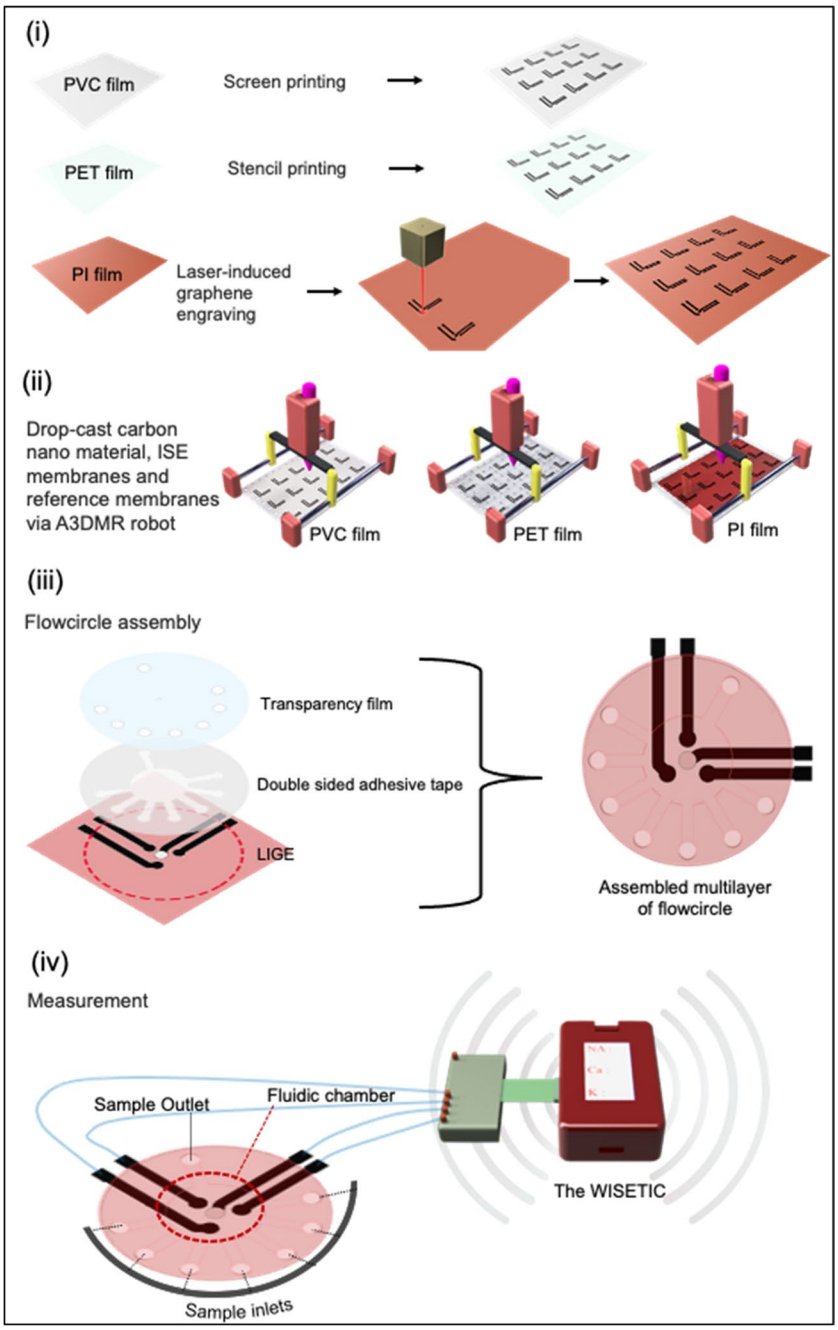

Fig. 1 Fabrication steps of the microfluidic ISE array

optimize ISM components (Table S1) for Ca^{2+}-ISE. The potentiometric responses of the Ca^{2+}-ISEs were tested in 10^{-5} – 10^{-1} M $CaCl_2$ solutions. Table S2 shows the sensitivity and limit of detection (LOD) of CB-modified all-solid-state electrodes at different ISM components after conditioning in 10^{-2} M $CaCl_2$ solution for overnight. The LODs were calculated according to the IUPAC definition via the intersection of extrapolated linear portions of the calibration curve [28, 29]. The results showed that the membrane M3 provides highest response slope with a Nernstian response of 29.8 ± 0.7 mV $decade^{-1}$ in the activity range from 10^{-4} to 10^{-1} M, and the LOD calculated as 10^{-5} M for Ca^{2+} detection. According to Table S2, the PVC membranes plasticized with NPOE showed the highest potentiometric response slope and the lowest LOD compared to DOS plasticized membranes (M5, M6 and M7), which is in agreement with literature [30, 31]. In addition, the ratio of 0.30 (additive to ionophore) with the increased amount of ionophore compared to the ISEs prepared with M1, M2 and M4 gave the highest response slope among membrane compositions including NPOE as the plasticizer and KTClPB as the additive, showing the

significant effect of the ionophore content in ISE membranes in the whole membrane mass [26].

Optimization of carbon-based material type and composition

After testing various ISM compositions, we investigated the effect of carbon-based material type and composition on ISE performance. Ca^{2+}-ISEs with CB, MWCNTs, GR and the CB mixtures with MWCNT or GR as intermediate layer were tested in 10^{-5} – 10^{-1} M Ca^{2+}. As shown in Fig. 2, the results showed that CB-modified Ca^{2+}-ISE provides higher sensitivities than unmodified Ca^{2+}-ISEs. This result demonstrated that the use of carbon material as an intermediate layer prevents the formation of an aqueous layer between the membrane and the transducer, thus improving sensitivity of the potentiometric signal [13, 32]. Moreover, the results indicate that CB- and MWCNTs-modified Ca^{2+}-ISEs exhibited high sensitivities while GR-modified Ca^{2+}-ISEs had lower sensitivities. Based on the results, the CB and MWCNTs have shown more stable dispersion on the electrode surface compared to GR without pretreatment, leading to improved adhesion between transducer and ISM [10, 33, 34]. Although MWCNT- and CB-modified ISEs exhibited similar potentiometric response, we chose CB to modify electrode surfaces since CB is less expensive than other carbon-based materials tested including MWCNTs. Moreover, EIS characterization of carbon-based material type and composition on Ca^{2+}-ISE is presented in Fig. S3 and Table S3. The smallest R_{ct} value was obtained with the CB-modified Ca^{2+}-ISE, verifying that the introduction of CB can improve the sensitivity of potentiometric response for ions measurement.

Optimization of substrate materials

For ISE fabrication, the substrate material type was optimized including PET, PVC, and PI. The electrode-based PET and PVC substrates were fabricated by screen-printing as screen-printed electrode (SPCE). While PI was used for laser scribing to create a LIGE and the optimization of LIGE fabrication was showed in Fig. S4 and Table S4. All-solid-state Ca^{2+}-ISEs prepared with 5 mg mL^{-1} CB and membrane M3 on PET, PVC, and PI substrates were tested with conditioning in 10^{-2} M $CaCl_2$ solution for overnight. As shown in Table S5, the obtained slopes of Ca^{2+}-ISEs fabricated with PET and PI are closer to the theoretical Nernstian slope when compared to those obtained for the electrode on PVC substrate. This is expected due to the highly hydrophobic nature of PET and PI substrates that can prevent the formation of a water layer between transducer and ISM, improving their potentiometric sensitivities for Ca^{2+} detection [35, 36]. In addition, the surface characterization and hydrophobic or hydrophilic nature of these substrates were investigated via FTIR as discussed in SI and shown in Figure S5. Therefore, the PET and PI substrates were chosen for the fabrication of ISEs.

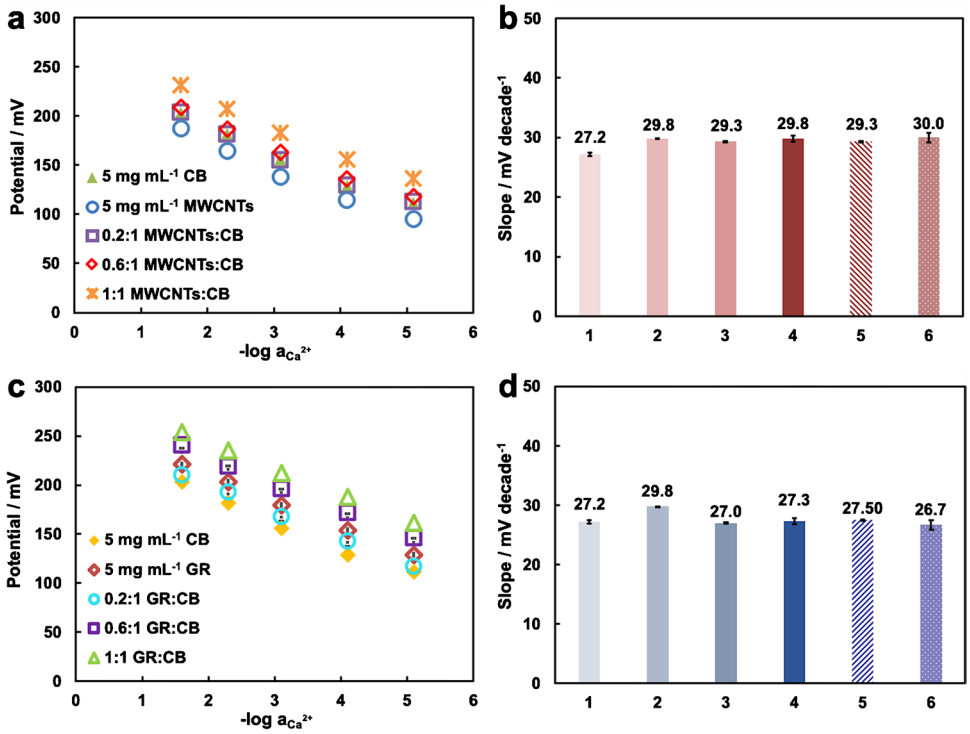

Fig. 2 Potentiometric responses of the Ca^{2+}-ISEs based on PET substrate at different carbon-based material type and composition (**a**) CB, MWCNTs and MWCNTs:CB (**c**) CB, GR and GR:CB. (**b**) Sensitivities of the Ca^{2+}-ISEs: (1) without intermediate layer, (2) 5 mg mL^{-1} CB, (3) 5 mg mL^{-1} MWCNTs, and the mixture ratio of MWCNTs and CB as (4) 0.2:1, (5) 0.6:1, and (6) 1:1, respectively. (**d**) Sensitivities of the Ca^{2+}-ISEs: (1) without intermediate layer, (2) 5 mg mL^{-1} CB, (3) 5 mg mL^{-1} GR, and the mixture ratio of GR and CB as (4) 0.2:1, (5) 0.6:1, and (6) 1:1, respectively

Physical characterization of CB and ISM modified electrodes

The surface morphologies of the CB-modified electrodes and the additionally ISM coated electrodes on PET and PI substrates were investigated by FE-SEM as shown in Fig. 3. For Ca^{2+}-ISE based PET substrate, the SEM image display a high surface roughness for unmodified electrode (Fig. 3a (i)), whereas CB showed more uniformity on the modified electrode (Fig. 3a (ii)). To obtain Ca^{2+}-ISE, the Ca^{2+}-ISM was deposited on the top of CB-modified electrode and the smooth surface was clearly observed (Fig. 3a (iii)). In addition, cross-section of SEM image was used to identify the thickness of Ca^{2+}-ISE based PET substrate (Fig. 3a (iv)). It was found to be 34.2 ± 1.3 µm for unmodified SPCE, 38.8 ± 0.8 µm for CB-modified SPCE, and 29.2 ± 1.7 µm for ISM coated SPCE.

For LIGE, the presence of sponge like structure could be observed as well as the previous reports, leading to a higher surface roughness [37]. As shown in Fig. 3b (i), the top view of PI film after CO_2 infrared laser under ambient condition clearly revealed highly porous graphene arranged in a parallel pattern on the PI substrate [38]. The results confirmed that laser engraving on the PI film generates highly porous multilayer graphene [27]. Moreover, Fig. 3b (ii) show that CB was uniformly modified on the LIGE surface. After Ca^{2+}-ISM coating, the smooth surface of the film formation was clearly obtained on the CB-modified LIGE (Fig. 3b (iii)). The thicknesses of each layer on LIGE were obtained by cross-section as shown in Fig. 3b (iv) with the values of

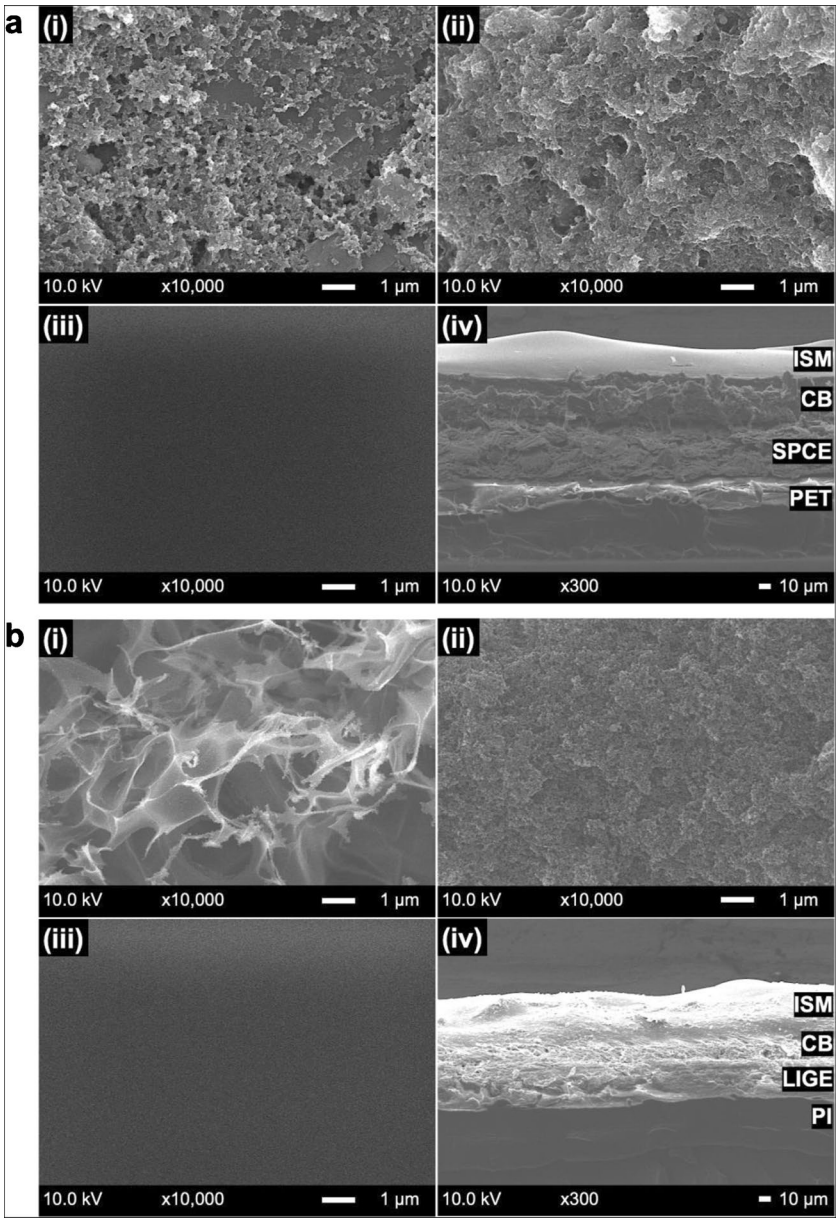

Fig. 3 FE-SEM images of (**a**) Ca^{2+}-ISE fabricated on PET substrate: (i) unmodified, (ii) CB- modified, and (iii) ISM/CB-modified electrodes and (iv) cross-section image of Fig. 3a (iii). (**b**) $Ca.^{2+}$-ISE fabricated on PI substrate: (i) unmodified, (ii) CB-modified, and (iii) ISM/CB-modified LIGEs and (iv) cross-section image of Fig. 3b (iii)

38.3 ± 0.3 µm for unmodified LIGE, 37.9 ± 1.6 µm for CB-modified LIGE, and 28.8 ± 1.1 µm for ISM coated LIGE.

In addition, the profile roughness (Ra) and area roughness (Sa) of the unmodified electrode and CB-modified electrode-based PET and PI substrates were investigated by laser confocal microscopy as shown in Fig. 4a and b. The results showed that the CB-modified electrode provides higher Ra and Sa than the unmodified SPCE and LIGE. These results demonstrated that the modification of CB increased the surface area of electrodes [39], leading to improved sensitivity of the potentiometric signal for ions detection.

Water layer and chronopotentiometry tests

The formation of water layer between the solid-contact and the ISM causes potential drift in ISEs [40]. Thus, the presence of an aqueous layer was tested for Ca^{2+}-ISE fabricated on PET and PI substrates as shown in Fig. 5. According to the Fig. 5a and b, CB-modified ISEs fabricated on both PI and PET substrates showed better potential stability compared to unmodified ISEs since there was no potential drift for the CB-modified Ca^{2+}-ISEs when changing the solution from primary ion (Ca^{2+}) to an interfering ion (Mg^{2+}). This could be explained by the highly hydrophobic nature of CB [12]. On the other hand, unmodified Ca^{2+}-ISEs showed 20 mV and 17 mV potential drift when the electrodes were introduced to 10^{-1} M $CaCl_2$ in the last step, indicating the existence of water layer. The contact angle measurements were carried out to investigate the hydrophobicity of the electrodes (Fig. 5c and d). The results showed that the contact angle of unmodified electrode based on PET and PI substrates was 89.9 ± 1.1° and 95.9 ± 3.7°, respectively. While CB-modified electrode had contact angles of 116.7 ± 2.6° and 126.1 ± 1.2° for PET and PI substrates, respectively. The results obtained clearly show that CB modification of electrode surface increased the hydrophobicity of the solid-contact material.

The short-term potential stability against polarization of the Ca^{2+}-ISEs modified with CB as intermediate layers were tested using chronopotentiometry with a constant current

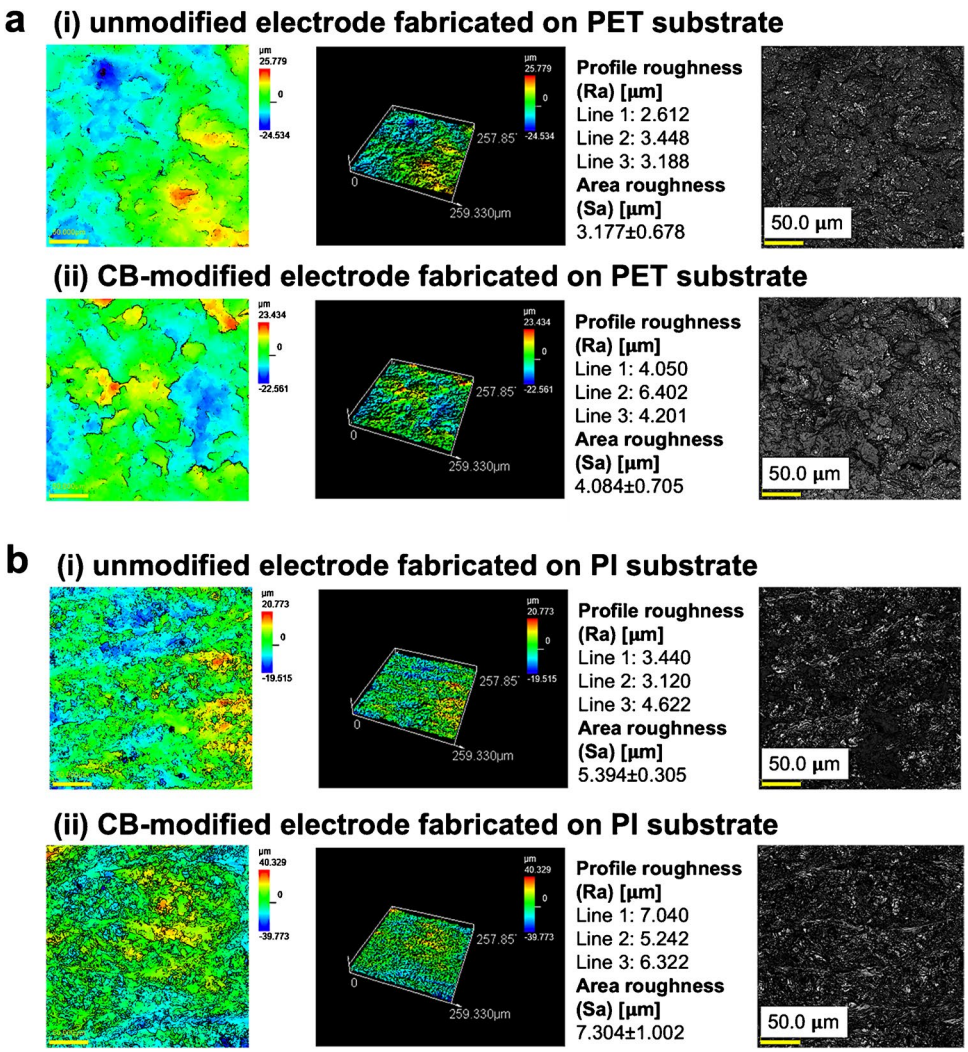

Fig. 4 LSCM images of (**a**) electrode fabricated on PET substrate: (i) unmodified, and (ii) CB-modified electrodes. (**b**) electrode fabricated on PI substrate: (i) unmodified, and (ii) CB-modified electrodes

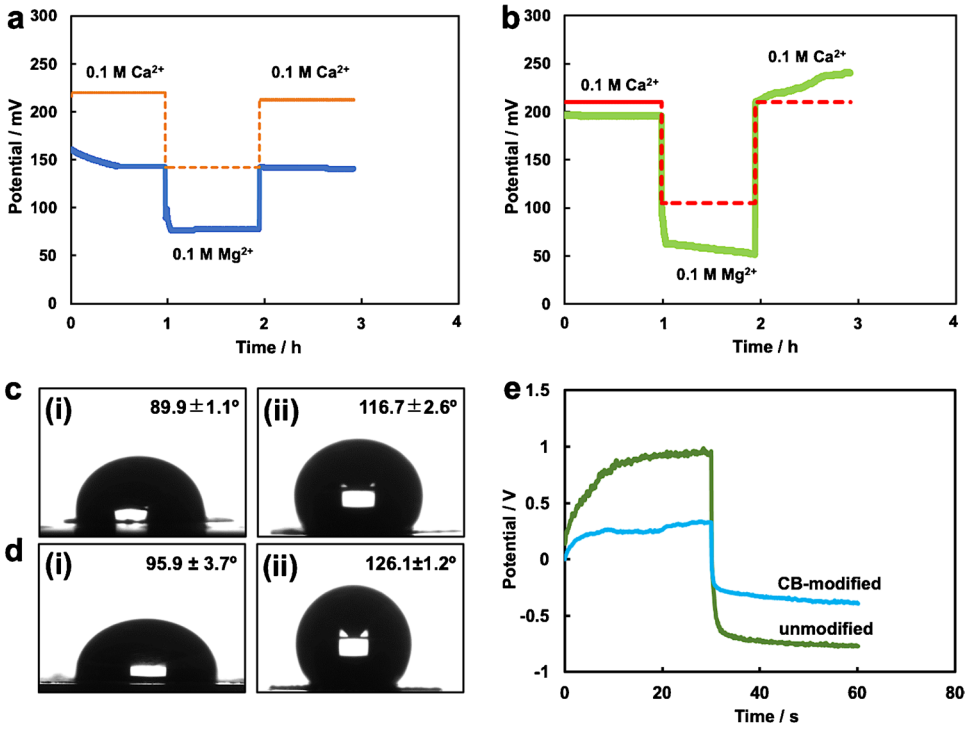

Fig. 5 **a**) Water layer tests of the unmodified (blue) and CB-modified (orange) Ca^{2+}-ISEs fabricated on PI substrate. **b**) Water layer tests of the unmodified (green) and CB-modified (red) Ca^{2+}-ISEs fabricated on PET substrate. **c**) and **d**) The contact angle measurements of (i) unmodified and (ii) CB-modified electrodes on PET and PI substrates, respectively. (**e**) Chronopotentiograms for the Ca^{2+}-ISEs prepared on PET substrate with unmodified and CB-modified electrodes measured in 10^{-1} $CaCl_2$ by applying + 1 nA for 30 s and then − 1 nA for 30 s

of ± 1 nA for 60 s in 10^{-1} M $CaCl_2$ [41]. The obtained chronopotentiograms are shown in Fig. 5e. The potential drift during cathodic and anodic polarization of the CB-modified Ca^{2+}-ISE was much lower than that obtained from the unmodified Ca^{2+}-ISE, indicating similar results with previous reports [24]. This effect is explained by the conductivity of the solid-contact materials used.

Response time, temperature and pH tests

The Ca^{2+}-ISE fabricated on PI substrate exhibited very fast response (< 1 s), the Ca^{2+}-ISE based on PET substrate had a response time of 10 s (Fig. 6a). The temperature test of the Ca^{2+}-ISE on both of PET and PI substrates was carried out in 1 mM Ca^{2+} (Fig. 6b). Potentiometric responses of the electrodes were constant between 35 − 40 ºC for $CaCl_2$. The effect of pH on the ISEs response were investigated in 10^{-3} M and 10^{-2} M $CaCl_2$ at pH 2 − 10 and is shown in Fig. 6c and d for PI and PET substrates, respectively. It was observed that there was no significant potential change between pH 4 − 9, showing a wide pH working range. The results demonstrated that the developed ISEs have wide working pH and body temperature range, which is important for the use as wearable devices.

Analytical performance of potentiometric devices

Potentiometric measurements were carried out in $10^{-6} - 10^{-1}$ M Na^+, K^+, Ca^{2+} solution *vs.* both commercial Ag/AgCl and all-solid-state reference electrode. The open-circuit potential curves for Na^+-ISE, K^+-ISE and Ca^{2+}-ISE are shown in Fig. 7. The Ca^{2+}-ISE showed a linear response range in $10^{-4} - 10^{-1}$ M with a sensitivity of 30.1 mV decade^{-1} ($R^2 = 0.9981$) and limit of detection (LOD) of 10^{-5} M (Fig. 7a and b). Also, the sensitivities obtained *vs.* commercial Ag/AgCl reference electrode were close to those obtained in the presence of all-solid-state reference electrode (28.9 mV decade^{-1} for Ca^{2+}-ISE), indicating reliable results. While the sensitivity of Na^+-LIGE was 42.9 mV decade^{-1} ($R^2 = 0.9903$) within linear range of $10^{-4} - 10^{-1}$ M Na^+ with LOD of 10^{-5} M (Fig. 7d and e), the sensitivity of K^+-LIGE was 38.03 mV decade^{-1} ($R^2 = 0.9873$) within linear range of $10^{-3} - 10^{-1}$ M K^+ with LOD of 10^{-4} M (Fig. 7g and h).

Since the reproducibility of the ISEs is critical for mass production, the electrode-to-electrode reproducibility was tested by extrapolating the linear portion in the activity range from $10^{-4} - 10^{-1}$ M of the calibration curve to 1.0 M Ca^{2+}. The standard deviations of $E°$ were obtained as 1.9 mV ($n = 5$) and 8.6 mV ($n = 6$) for PET and PI substrate based Ca^{2+}-ISEs, respectively, showing better reproducibility with the CB/Ca^{2+}-ISE fabricated on PET substrate than those fabricated on PI substrate. Also, the standard deviation of $E°$ obtained for CB/Ca^{2+}-ISE based on PET is lower than those previous reports for platinum nanoparticles (4.6 mV) [42] or KTCNQ (5.7 mV) or NaTCNQ (5.1 mV) contacted electrodes [43] and comparable to those observed for electrodes with solid contact made of CB (1.1 mV) [44] or platinum nanoparticles-CB composite (1.4 mV) [45]. Although ISEs fabricated on PET substrate via in-house stencil printing gives better

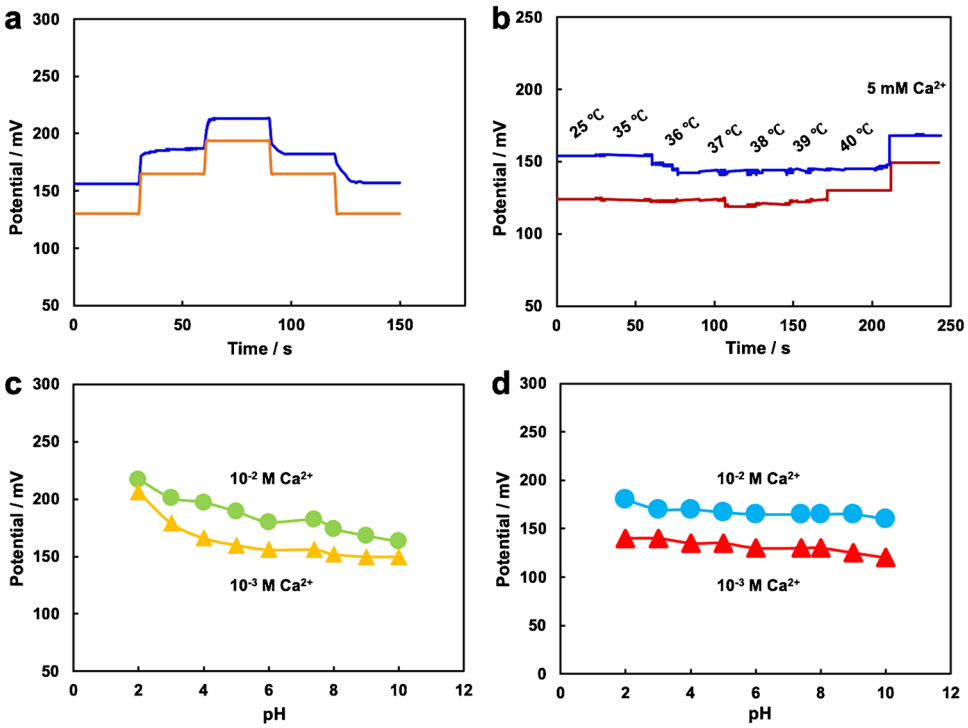

Fig. 6 **a**) Response time of the Ca^{2+}-ISEs fabricated on PI (orange line) and PET (blue line) substrates. **b**) The effect of temperature on the potential response of the Ca^{2+}-ISEs fabricated on PI (red line) and PET (blue line) substrates, the signal is measured every 10 °C from 25 °C to 40 °C in 10^{-3} M Ca^{2+}. The effect of pH on the Ca^{2+}-ISEs for (**c**) PI and, (**d**) PET substrates

reproducibility than CB/Ca^{2+}-ISE fabricated on PI substrate via laser-engraving, LIGEs have advantage in that they are easily mass-produced via automated system. Also, the standard deviation of $E°$ obtained for LIGEs (8.6 mV) is comparable with other reports (0.7–32.2 mV) [46].

For repeatability study of the ISEs, the ISEs were repeatedly used in 1 mM and 5 mM Ca^{2+}, 1 mM and 100 mM Na^+, and 5 mM and 50 mM K^+ and, the potential responses are shown in Fig. 7c, f and i. As can be seen, the potential was the same for each corresponding activity after several cycles, indicating that the developed ISEs had good repeatability. In addition, the selectivity was also studied and is shown in Table S10.

The stability of the ISEs was investigated over 30 days by measuring the slope and LOD. The ISEs were stored at room temperature and were conditioned in 10^{-1} M for Na^+ or K^+ and 10^{-2} M for Ca^{2+} prior to use. The obtained slopes of Na^+ or K^+, and Ca^{2+} were 42.7 ± 0.2 mV decade^{-1}, 37.8 ± 0.4 mV decade^{-1}, and 28.7 ± 0.2 mV decade^{-1}, respectively. The observed changes in the slopes were less than 5 mV decade^{-1}, showing the high stability of the proposed potentiometric sensors.

The comparison of our approach versus other ISEs including potentiometric and optical methods for determination of ions in biological fluid is summarized in Table S7. Although the linear range and LODs found in this work is comparable, the conductive material used in those works presented (Table S7) are either expensive or affected by light/oxidation, decreasing their stability. In addition, their fabrication process includes complicated and manual steps, indicating that our system could be promising to detect ions in complex biological fluids such as urine and sweat.

Sample analysis

To demonstrate the clinical applicability of the sensing platform, we tested real urine and simulated sweat samples by filling the microfluidic channels of the ISE array and using the portable and wireless potentiometer with its customized software (the details of synchronization algorithms are presented in Figure S6). Different concentrations of KCl, NaCl and $CaCl_2$ in the physiologically relevant range in a background of simulated sweat were prepared and the developed ISEs were used to obtain the calibration curves. The potential responses in varying activity of primary ions for Na^+, K^+ and Ca^{2+} in simulated sweat are summarized in Table S8.

In addition, the applicability of the microfluidic devices was investigated by measuring the concentration of Na^+, K^+ and Ca^{2+} in real human urine. In detail, urine samples were diluted 20 times with 10 mM HEPES (pH 7.4) before analysis with the microfluidic devices, and the results were validated using ICP-OES method. As shown in Table S9-S11, the measured concentrations were not statistically different from those obtained by ICP-OES, verifying the possibility of accurate measurements using our proposed microfluidic device.

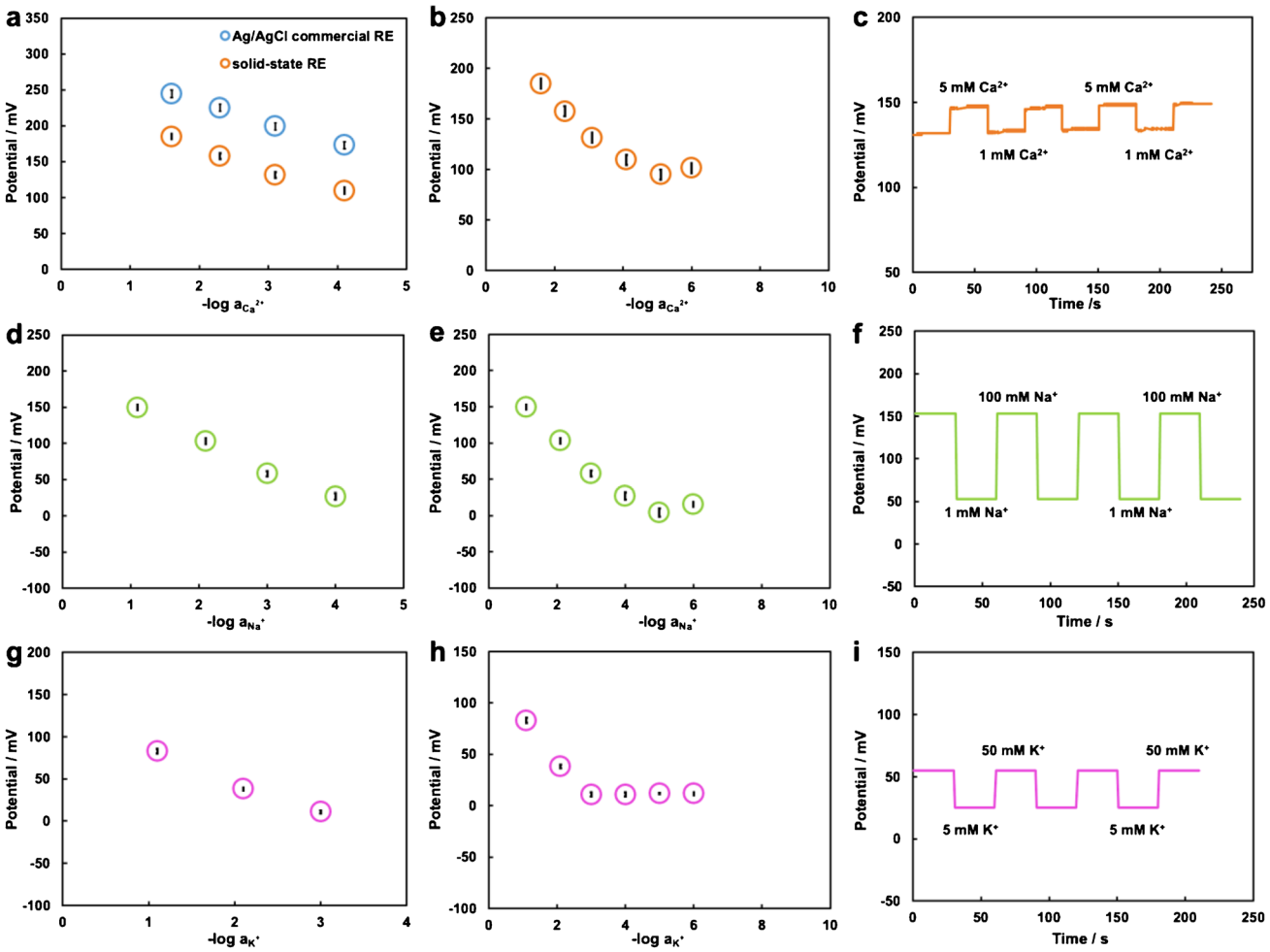

Fig. 7 **a**) Calibration curves in $10^{-4}-10^{-1}$ M Ca^{2+}, (**b**) detection limit, and (**c**) repeatability of the Ca^{2+}-ISEs in 1 mM and 5 mM Ca^{2+}. (**d**) Calibration curves in $10^{-4}-10^{-1}$ M Na^+, (**e**) detection limit, and (**f**) repeatability of the Na^+-ISEs in 1 mM and 100 mM Na^+. **g**) calibration curves in $10^{-3}-10^{-1}$ M K^+, (**h**) detection limit, and (**i**) repeatability of the K^+-ISEs in 5 mM and 50 mM K^+

Conclusions

Here, we presented the large-scale fabrication of LIGEs for multiplexed detection of Na^+, K^+, and Ca^{2+} in urine and sweat samples at the POC. The manufacturing system offers low-cost, rapid, and automated construction of ISE arrays. PVC, PET, and PI were used as substrates for ISEs fabrication and compared in terms of their sensitivities. Then, CB was selected to modify electrode surface for improved electrode characteristics. Moreover, an automated custom-made 3D-printed dispensing robot namely A3DMR was used to achieve drop-cast steps for ISE fabrication by eliminating manual steps. All of the sensors showed good sensitivity, selectivity, and reproducibility, making the ISEs suitable for sample analysis. Also, the custom-made miniaturized potentiometer was used for signal collection and wireless signal transmission to a smartphone with a customized software for POC application. The device is able to simultaneously detect Na^+, K^+, and Ca^{2+} ions in human urine and simulated sweat samples. Mass production of the ISEs will enable low-cost analysis of electrolytes and can be expanded for other ions and metabolites for future clinical applications to monitor physiological conditions. Due to the use of IoT supported miniaturized potentiometer, big data could be collected at home-tests and stored in servers to provide medical information about patients for early and rapid diagnosis, and proper treatment by doctors especially during pandemic situations.

Supplementary information The online version contains supplementary material available at https://doi.org/10.1007/s00604-023-05818-8.

Acknowledgements Kanyapat Teekayupak gratefully thanks to the 100th Anniversary Chulalongkorn University Fund for Doctoral Scholarship. This research was supported by National Research Council of Thailand (NRCT5-TRG63001-02). Additional support was provided by The Scientific and Technological Research Council of Turkey (TUBITAK) 122Z721 and 120N615. The author also gratefully acknowledges SciSpec Co., Ltd. for validation method with ICP-OES and Metabolic

Disease in Gastrointestinal and Urinary System Research Unit, Department of Biochemistry, Faculty of Medicine, Chulalongkorn University for urine samples.

Author contribution Kanyapat Teekayupak: Formal analysis, Investigation, Methodology, Writing—Original Draft. Atchara Lomae: Formal analysis, Methodology, Writing—Original Draft. Ismail Agir: Investigation, Methodology, Software, Writing—Review & Editing. Natthaya Chuaypen: Real sample resource. Thasinas Dissayabutra: Real sample resource. Charles S. Henry: Investigation, Visualization, Writing—Review & Editing. Orawon Chailapakul: Investigation, Supervision. Tugba Ozer: Conceptualization, Supervision, Visualization, Writing—Review & Editing. Nipapan Ruecha: Conceptualization, Project administration, Supervision, Visualization, Writing—Review & Editing.

Data Availability The datasets generated during and/or analyzed during the current study are available from the correspondingauthor on reasonable request.

Declarations

Competing interest The authors declare that they have no known competing financial interests or personal relationships that could have appeared to influence the work reported in this paper.

References

1. Bagheri N, Mazzaracchio V, Cinti S, Colozza N, Di Natale C, Netti PA et al (2021) Electroanalytical sensor based on gold-nanoparticle-decorated paper for sensitive detection of copper ions in sweat and serum. Anal Chem 93:5225–5233
2. di Sant'Agnese PA, Darling RC, Perera GA, Shea E (1953) Abnormal electrolyte composition of sweat in cystic fibrosis of the pancreas: clinical significance and relationship to the disease. Pediatrics 12:549–563
3. Mahendran V, Philip J (2013) Sensing of biologically important cations such as Na^+, K^+, Ca^{2+}, Cu^{2+}, and Fe^{3+} using magnetic nanoemulsions. Langmuir 29:4252–4258
4. Riccardi D, Kemp PJ (2012) The calcium-sensing receptor beyond extracellular calcium homeostasis: conception, development, adult physiology, and disease. Annu Rev Physiol 74:271–297
5. Lehnhardt A, Kemper MJ (2011) Pathogenesis, diagnosis and management of hyperkalemia. Pediatr Nephrol 26:377–384
6. Donaldson SH, Boucher RC (2007) Sodium channels and cystic fibrosis. Chest 132:1631–1636
7. Adams J, Badolato M, Pierce E, Cantrell A, Parker Z, Farzam D (2021) Short-Term Stability of Urine Electrolytes: Effect of Time and Storage Conditions. Int J Sport Nutr Exerc Metab 1:1–3
8. Bobacka J, Ivaska A, Lewenstam A (2008) Potentiometric ion sensors. Chem Rev 108:329–351
9. Soda Y, Citterio D, Bakker E (2019) Equipment-free detection of K^+ on microfluidic paper-based analytical devices based on exhaustive replacement with ionic dye in ion-selective capillary sensors. ACS sensors 4:670–677
10. Shao Y, Ying Y, Ping J (2020) Recent advances in solid-contact ion-selective electrodes: Functional materials, transduction mechanisms, and development trends. Chem Soc Rev 49:4405–4465
11. Yin T, Qin W (2013) Applications of nanomaterials in potentiometric sensors. TrAC, Trends Anal Chem 51:79–86
12. Paczosa-Bator B (2012) All-solid-state selective electrodes using carbon black. Talanta 93:424–427
13. Ozer T, Henry CS (2022) All-solid-state potassium-selective sensor based on carbon black modified thermoplastic electrode. Electrochim Acta 404:139762
14. Crespo GA, Gugsa D, Macho S, Rius FX (2009) Solid-contact pH-selective electrode using multi-walled carbon nanotubes. Anal Bioanal Chem 395:2371–2376
15. Ping J, Wang Y, Wu J, Ying Y (2011) Development of an all-solid-state potassium ion-selective electrode using graphene as the solid-contact transducer. Electrochem Commun 13:1529–1532
16. Bobacka J (2006) Conducting polymer-based solid-state ion-selective electrodes. Electroanalysis 18:7–18
17. Manjushree S, Adarakatti PS (2023) Recent advances in disposable electrochemical sensors. In: recent developments in green electrochemical sensors: design, performance, and applications. Am Chem Soc pp 1–21
18. Hjort RG, Soares RR, Li J, Jing D, Hartfiel L, Chen B et al (2022) Hydrophobic laser-induced graphene potentiometric ion-selective electrodes for nitrate sensing. Microchim Acta 189:122
19. Lee C-W, Jeong S-Y, Kwon Y-W, Lee J-U, Cho S-C, Shin B-S (2022) Fabrication of laser-induced graphene-based multifunctional sensing platform for sweat ion and human motion monitoring. Sens Actuators A 334:113320
20. Liao J, Zhang X, Sun Z, Chen H, Fu J, Si H et al (2022) Laser-induced graphene-based wearable epidermal ion-selective sensors for noninvasive multiplexed sweat analysis. Biosensors 12:397
21. van de Velde L, d'Angremont E, Olthuis W (2016) Solid contact potassium selective electrodes for biomedical applications–a review. Talanta 160:56–65
22. Ozer T, Agir I, Henry CS (2022) Rapid prototyping of ion-selective electrodes using a low-cost 3D printed internet-of-things (IoT) controlled robot. Talanta 247:123544
23. Ozer T, Agir I, Henry CS (2022) Low-cost Internet of Things (IoT)-enabled a wireless wearable device for detecting potassium ions at the point of care. Sens Actuators B Chem 365:131961
24. Ozer T, Henry CS (2022) Microfluidic-based ion-selective thermoplastic electrode array for point-of-care detection of potassium and sodium ions. Microchim Acta 189:1–12
25. Ozer T (2022) Carbon composite thermoplastic electrodes integrated with mini-printed circuit board for wireless detection of calcium ions. Anal Sci 38:1233–1243
26. Mikhelson KN (2013) Ionophore-Based ISEs. Springer, Ion-Selective Electrodes, pp 51–95
27. Lin J, Peng Z, Liu Y, Ruiz-Zepeda F, Ye R, Samuel EL et al (2014) Laser-induced porous graphene films from commercial polymers. Nat Commun 5:1–8
28. McNaught AD, Wilkinson A (1997)Compendium of chemical terminology. Blackwell Science, London
29. Bakker E, Pretsch E (2005) Potentiometric sensors for trace-level analysis. TrAC, Trends Anal Chem 24:199–207
30. Bakker E, Bühlmann P, Pretsch E (1997) Carrier-based ion-selective electrodes and bulk optodes. 1. General characteristics. Chem Rev 97:3083–132
31. Bühlmann P, Pretsch E, Bakker E (1998) Carrier-based ion-selective electrodes and bulk optodes. 2. Ionophores for potentiometric and optical sensors. Chem Rev 98:1593–688
32. Mazzaracchio V, Serani A, Fiore L, Moscone D, Arduini F (2021) All-solid state ion-selective carbon black-modified printed electrode for sodium detection in sweat. Electrochim Acta 394:139050
33. Pięk M, Piech R, Paczosa-Bator B (2016) The complex crystal of NaTCNQ–TCNQ supported on different carbon materials as ion-to-electron transducer in all-solid-state sodium-selective electrode. J Electrochem Soc 163:B573

34. Kang YJ, Chung H, Kim M-S, Kim W (2015) Enhancement of CNT/PET film adhesion by nano-scale modification for flexible all-solid-state supercapacitors. Appl Surf Sci 355:160–165
35. Rostampour M, Lawrence Jr DJ, Hamid Z, Darensbourg J, Calvo-Marzal P, Chumbimuni-Torres KY (2023) Highly reproducible flexible ion-selective electrodes for the detection of sodium and potassium in artificial sweat. Electroanalysis 35:2200121
36. Choudhury S, Roy S, Bhattacharya G, Fishlock S, Deshmukh S, Bhowmick S et al (2021) Potentiometric ion-selective sensors based on UV-ozone irradiated laser-induced graphene electrode. Electrochim Acta 387:138341
37. Cinti S, Mazzaracchio V, Cacciotti I, Moscone D, Arduini F (2017) Carbon black-modified electrodes screen-printed onto paper towel, waxed paper and parafilm M®. Sensors 17:2267
38. Wan Z, Umer M, Lobino M, Thiel D, Nguyen N-T, Trinchi A et al (2020) Laser induced self-N-doped porous graphene as an electrochemical biosensor for femtomolar miRNA detection. Carbon 163:385–394
39. Lee J-H, Wee S-B, Kwon M-S, Kim H-H, Choi J-M, Song MS et al (2011) Strategic dispersion of carbon black and its application to ink-jet-printed lithium cobalt oxide electrodes for lithium ion batteries. J Power Sources 196:6449–6455
40. De Marco R, Veder J-P, Clarke G, Nelson A, Prince K, Pretsch E et al (2008) Evidence of a water layer in solid-contact polymeric ion sensors. Phys Chem Chem Phys 10:73–76
41. Bobacka J (1999) Potential stability of all-solid-state ion-selective electrodes using conducting polymers as ion-to-electron transducers. Anal Chem 71:4932–4937
42. Paczosa-Bator B, Cabaj L, Piech R, Skupień K (2012) Platinum nanoparticles intermediate layer in solid-state selective electrodes. Analyst 137:5272–5277
43. Paczosa-Bator B, Pięk M, Piech R (2015) Application of nanostructured TCNQ to potentiometric ion-selective K^+ and Na^+ electrodes. Anal Chem 87:1718–1725
44. Paczosa-Bator B (2014) Effects of type of nanosized carbon black on the performance of an all-solid-state potentiometric electrode for nitrate. Microchim Acta 181:1093–1099
45. Paczosa-Bator B, Cabaj L, Piech R, Skupień K (2013) Potentiometric sensors with carbon black supporting platinum nanoparticles. Anal Chem 85:10255–10261
46. Rousseau CR, Bühlmann P (2021) Calibration-free potentiometric sensing with solid-contact ion-selective electrodes. TrAC, Trends Anal Chem 140:116277